Journal of Alloys and Compounds 437 (2007) 120–126

Journal of ALLOYS AND COMPOUNDS

www.elsevier.com/locate/jallcom

Internal friction of R-phase and B19′ martensite in equiatomic TiNi shape memory alloy under isothermal conditions

S.H. Chang, S.K. Wu *

Department of Materials Science and Engineering, National Taiwan University, Taipei 106, Taiwan

Received 6 May 2006; received in revised form 19 July 2006; accepted 19 July 2006
Available online 6 September 2006

Abstract

The intrinsic internal friction IF_I of R-phase and B19′ martensite are composed of static internal friction IF_S and dynamic internal friction IF_D. The tan δ values of IF_S^R and $IF_S^{B19'}$ are both proportional to $\sigma_0/\upsilon^{1/2}$ and are related to the stress-assisted motions of twin boundaries. The tan δ values of IF_S^R are higher than those of $IF_S^{B19'}$ is owing to the softer storage modulus E_0 in R-phase. The tan δ values of $IF_D^{B19'}$ are linearly proportional to $\dot{T}/\upsilon^{1/2}$. The occurrence of relaxation peak at ≈−60 °C is found to come from the $IF_S^{B19'}$, instead of the $IF_D^{B19'}$.

Keywords: Shape memory alloy; Thermal (dynamic mechanical) analysis; Internal friction; Martensite

1. Introduction

TiNi alloys are known as important shape memory alloys (SMAs) because of their functional properties such as shape memory effect and superelasticity [1]. Many reported studies revealed that TiNi SMAs exhibit a high internal friction peak associated with a shear modulus minimum during martensitic transformation and thus are suitable for the energy dissipation applications [2–9]. The damping characteristics of internal friction peak during martensitic transformation are associated with experimental parameters such as temperature rate $\dot{T}$, frequency υ and amplitude σ_0. It is also reported that both R-phase premartensite and B19′ martensite in TiNi SMAs perform a high damping property due to the easy movement of their twin boundaries in between the variants [5]. Besides, the occurrence of R-phase can strongly soften the storage modulus E_0 and thus promotes the TiNi SMAs' damping capacity [10]. In addition to the internal friction peaks in TiNi SMAs, there is also a relaxation peak appearing at temperature around 200 K. Iwasaki and Hasiguti [2] proposed that this relaxation peak is thermally activated and originates from dislocations.

It has been proposed that the internal friction of a first-order phase transformation can be decomposed into three terms: IF_{Tr}, IF_{PT} and IF_I [11–17]. The first term IF_{Tr} is the transitory internal friction which appears only at low υ and non-zero $\dot{T}$. It depends on external parameters such as $\dot{T}$, υ, σ_0 and volume fraction transformed per unit time. The second term IF_{PT} is the internal friction due to the phase transformation, but it does not depend on $\dot{T}$. The third term IF_I is the intrinsic internal friction of austenitic or martensitic phase measured at constant $\dot{T}$ and strongly dependent on microstructure properties such as dislocations, vacancies and twin boundaries. In the low frequency range, the internal friction peak observed during transformation is mainly ascribed to the first term IF_{Tr}. In equiatomic TiNi SMA, Chang and Wu [18] reported that the inherent internal friction ($IF_{PT} + IF_I$) measured under isothermal conditions during B2 → R and R → B19′ martensitic transformation are linearly proportional to $\sigma_0/\upsilon^{1/2}$ but independent of $\dot{T}$. The damping mechanism of the inherent internal friction ($IF_{PT} + IF_I$) is mainly generated from the stress-assisted martensitic transformation and stress-assisted motions of twin boundaries. However, all the reported studies focus on the damping characteristics of transitory and inherent internal friction (IF_{Tr}, IF_I or $IF_{PT} + IF_I$) during martensitic transformation. The damping characteristics of the single phase in TiNi SMAs, such as B2 parent phase, R-phase premartensite and B19′ martensite, under isothermal conditions have not been systematically studied before. In this study, the damping capacity tan δ values of a $Ti_{50}Ni_{50}$ SMA which exhibits a two-stage B2 → R → B19′ martensitic transformation during cooling are measured by dynamic mechanical

* Corresponding author. Tel.: +886 2 2363 7846; fax: +886 2 2363 4562.
E-mail address: skw@ntu.edu.tw (S.K. Wu).

0925-8388/$ – see front matter © 2006 Elsevier B.V. All rights reserved.
doi:10.1016/j.jallcom.2006.07.092

analyzer (DMA) under isothermal conditions at different temperatures. Thereafter, the isothermal damping characteristics of each single phase: B2, R-phase and B19′ martensite are discussed.

2. Experimental procedures

Equiatomic $Ti_{50}Ni_{50}$ alloy was prepared by conventional vacuum arc remelting. The as-melted ingot was hot-rolled at 850 °C into a 2 mm thick plate and then the plate was solution-treated at 850 °C for 2 h followed by quenching in water. Then, the plate was cold-rolled at room temperature along the hot-rolling direction and reached a final 30% thickness reduction. Subsequently, the cold-rolled plate was cut into test specimens with the dimension of 40 mm × 5 mm × 1.26 mm, sealed in an evacuated quartz tube and annealed at 650 °C for 2 min. The detailed procedure for preparing specimen is demonstrated in another paper [18].

Transformation temperatures of cold-rolled and annealed specimen were determined by differential scanning calorimetry (DSC) test using a TA Q10 DSC equipment with a constant cooling rate of 10 °C/min. Specimen for DMA experiment was cut along the rolling direction to eliminate the influence of rolling texture [19]. The tan δ and storage modulus E_0 were measured by a TA 2980 DMA equipment using a constant cooling rate of 3 °C/min. The isothermal damping characteristics of B2, R-phase and B19′ martensite were also investigated by DMA but tested under isothermal conditions using various amplitudes and frequencies. The detailed procedure for the isothermal DMA test was conducted as follows. The specimen was initially cooled starting from 150 °C at a constant cooling rate (1, 3 or 5 °C/min) and was kept isothermally for 30 min at the set temperature. After being isothermal for 30 min, the specimen was heated up to 150 °C to ensure it had returned to B2 parent phase. Then, the specimen was cooled to another set temperature and kept isothermally at that temperature for 30 min. During the isothermal conditions, the set temperature was chosen in between +80 °C and −80 °C in which B2, R-phase and B19′ martensite are all included.

3. Experimental results

3.1. DSC and DMA measurements at constant $\dot{T}$

Fig. 1 shows the DSC and DMA curves of 30% cold-rolled $Ti_{50}Ni_{50}$ alloy annealed at 650 °C for 2 min. As shown in Fig. 1, there are two transformation peaks, i.e. B2 → R and R → B19′ obtained in DSC cooling curve. There are also two transformation peaks appearing in the tan δ curve which correspond to B2 → R and R → B19′ transformation peaks in DSC curve. Except the aforementioned tan δ transformation peaks, an extra broad peak which is not observed in DSC curve appears at about −65 °C in tan δ curve. This extra broad peak is

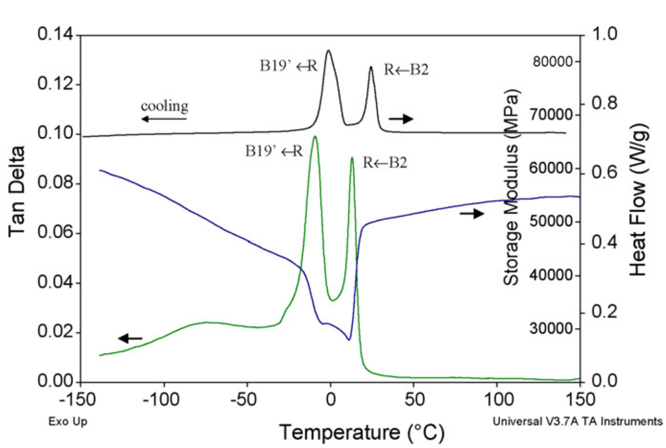

Fig. 1. DSC curve measured at $\dot{T} = 10$ °C/min and DMA curves measured at $\dot{T} = 1$ °C/min, $\upsilon = 1$ Hz and $\sigma_0 = 5$ µm for 30% cold-rolled $Ti_{50}Ni_{50}$ alloy annealed at 650 °C for 2 min.

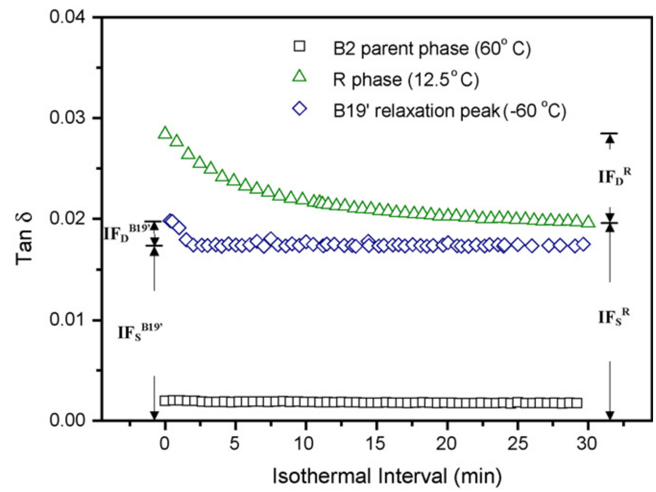

Fig. 2. The tan δ values vs. isothermal interval for Fig. 1 specimen measured at $\upsilon = 1$ Hz, $\sigma_0 = 5$ µm. The selected isothermal temperatures are 60 °C (B2 phase), 12.5 °C (R-phase) and −60 °C (B19′ martensite).

known as the relaxation peak [2,4]. Also from Fig. 1, the E_0 curve declines gently in B2 parent phase while cooling, then drops drastically and exhibits a deeper minimum during B2 → R transformation and a shallower minimum during R → B19′ transformation. After R → B19′ transformation completes, the E_0 value of B19′ martensite increases quickly with decreasing temperature.

3.2. DMA measurement under isothermal conditions

Fig. 2 plots the tan δ values versus isothermal interval when the specimen of Fig. 1 is tested by DMA under isothermal treatment at 60 °C (B2 parent phase), 12.5 °C (R-phase) and −60 °C (B19′ martensite) for 0–30 min. As shown in Fig. 2, the measured tan δ values of B2 parent phase are almost the same in the whole isothermal conditions. However, both the measured tan δ values of R-phase and B19′ martensite decrease with increasing isothermal intervals and reach a steady value after 10–15 min. As illustrated in Fig. 2, the tan δ values of R-phase and B19′ martensite are composed of a dynamic term IF_D which diminishes during isothermal conditions and a static term IF_S which is the steady value measured after 30 min of isothermal interval.

In order to investigate the damping characteristics of IF_S and IF_D for B2, R-phase and B19′ martensite under isothermal conditions, DMA tan δ tests under 30 min isothermal interval at different temperatures were conducted with various $\dot{T}$, υ, σ_0 and the results are exhibited in Figs. 3–5, respectively. Fig. 3(a)–(c) show the tan δ curves (empty mark curves) measured after 30 min isothermal interval at different temperatures when the specimen is conducted at the cooling rate $\dot{T}$ of 1, 3 and 5 °C/min, respectively, before it reaches the set isothermal temperature. The solid lines in Fig. 3(a)–(c) represent the tan δ curves measured at constant $\dot{T}$ of 1, 3 and 5 °C/min, respectively. Fig. 4(a)–(c) show the tan δ curves measured after 30 min isothermal condition (empty mark curves) at different υ of 0.1, 1 and 10 Hz, respectively. Fig. 5(a)–(c) are the tan δ curves measured after 30 min isothermal condition (empty mark curves) at different σ_0 of 5, 10 and 15 µm, respectively. In Figs. 4 and 5, the tan δ curves measured at constant $\dot{T}$ (solid line curves, $\dot{T} = 1$ °C/min) are also plotted for comparison. As shown in Figs. 3–5, all the tan δ values of B2 parent phase measured after isothermal conditions, i.e. IF_S^{B2}, are quite low and approximately same as those measured at constant $\dot{T}$ (IF_I^{B2}). The tan δ values of R-phase measured after isothermal conditions, i.e. IF_S^{R}, are much higher than those of IF_I^{B2}. However, the tan δ values of B19′ martensite measured after isothermal conditions, i.e. $IF_S^{B19'}$, decline quickly after R → B19′ transformation completes. With further isothermal treatment at lower temperatures, the tan δ values of $IF_S^{B19'}$ also exhibit a relaxation peak at around −60 °C. Fig. 6 enlarges the diagram of B19′ martensite region in Fig. 3(a) so to describe the decayed and steady tan δ values measured under isothermal conditions. As illustrated in Fig. 6, the intrinsic internal friction IF_IB19′ of B19′ martensite measured at constant $\dot{T}$ is composed of $IF_S^{B19'}$ and $IF_D^{B19'}$.

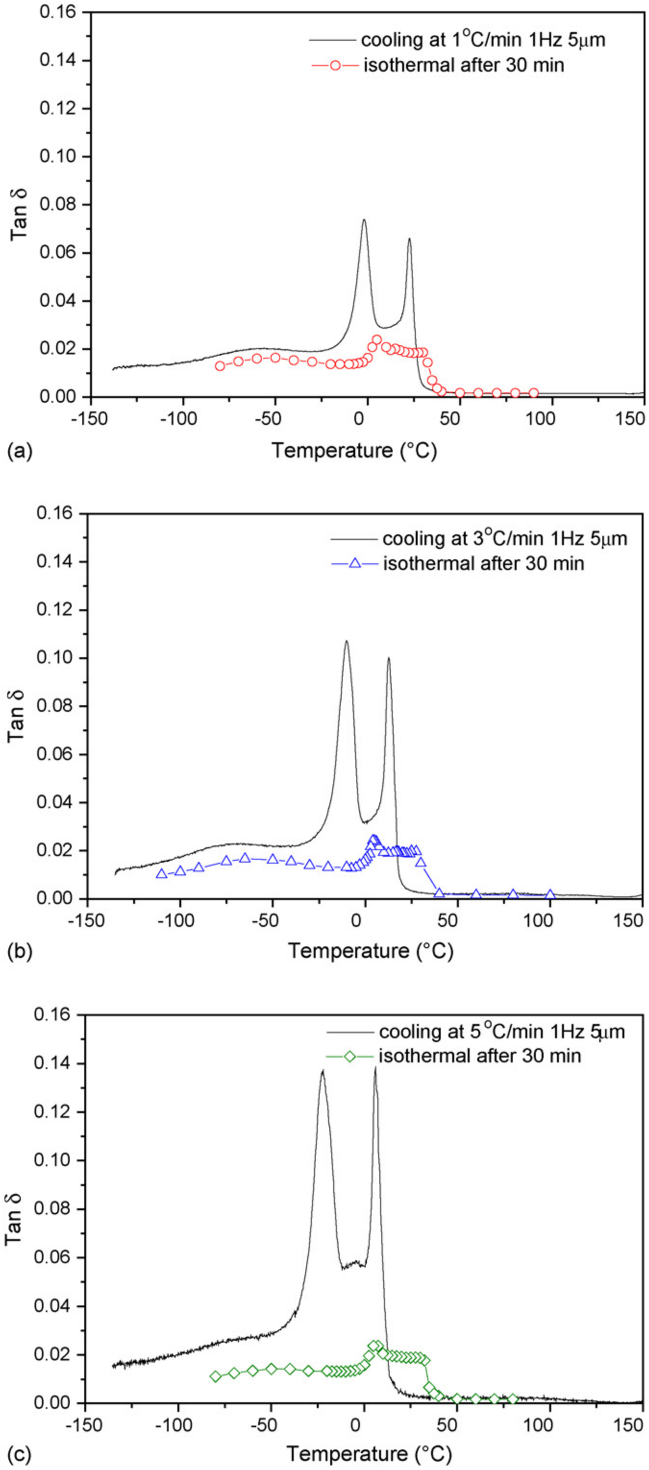

Fig. 3. The intrinsic tan δ curves measured under isothermal conditions at $\upsilon = 1$ Hz and $\sigma_0 = 5$ μm with different cooling rates of (a) $\dot{T} = 1\,^{\circ}\mathrm{C/min}$ (empty circle curve); (b) $\dot{T} = 3\,^{\circ}\mathrm{C/min}$ (empty triangle curve); and (c) $\dot{T} = 5\,^{\circ}\mathrm{C/min}$ (empty diamond curve).

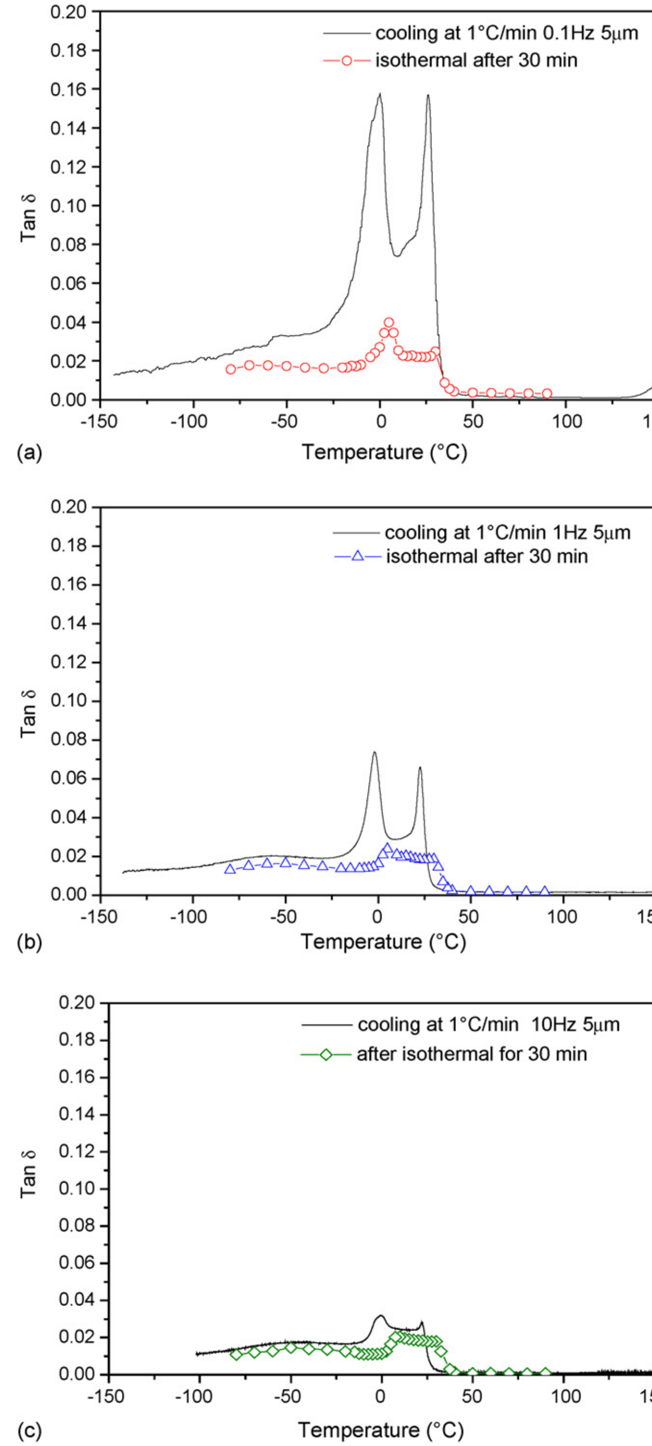

Fig. 4. The intrinsic tan δ curves measured under isothermal conditions at $\dot{T} = 1\,^{\circ}\mathrm{C/min}$ and $\sigma_0 = 5$ μm with different frequencies of (a) $\upsilon = 0.1$ Hz (empty circle curve); (b) $\upsilon = 1$ Hz (empty triangle curve); and (c) $\upsilon = 10$ Hz (empty diamond curve).

4. Discussion

4.1. IF_S of B2 parent phase, R-phase and B19′ martensite

From the DMA results exhibited in Figs. 3–5, all the internal friction of IF_S^{B2} are very low and their tan δ values associated with $\dot{T}$, υ and σ_0 are inconspicuous to investigate. Thus, only the effects of $\dot{T}$, υ and σ_0 on IF_S^{R} and $IF_S^{B19'}$ are discussed in the following. Fig. 7(a) plots the tan δ values of IF_S^{R} and $IF_S^{B19'}$ as a function of $\dot{T}$ measured at 20 °C and −20 °C, respectively, in Fig. 3. From Fig. 7(a), both the tan δ values of IF_S^{R} and $IF_S^{B19'}$ almost keep constant when measured at different $\dot{T}$. This fea-

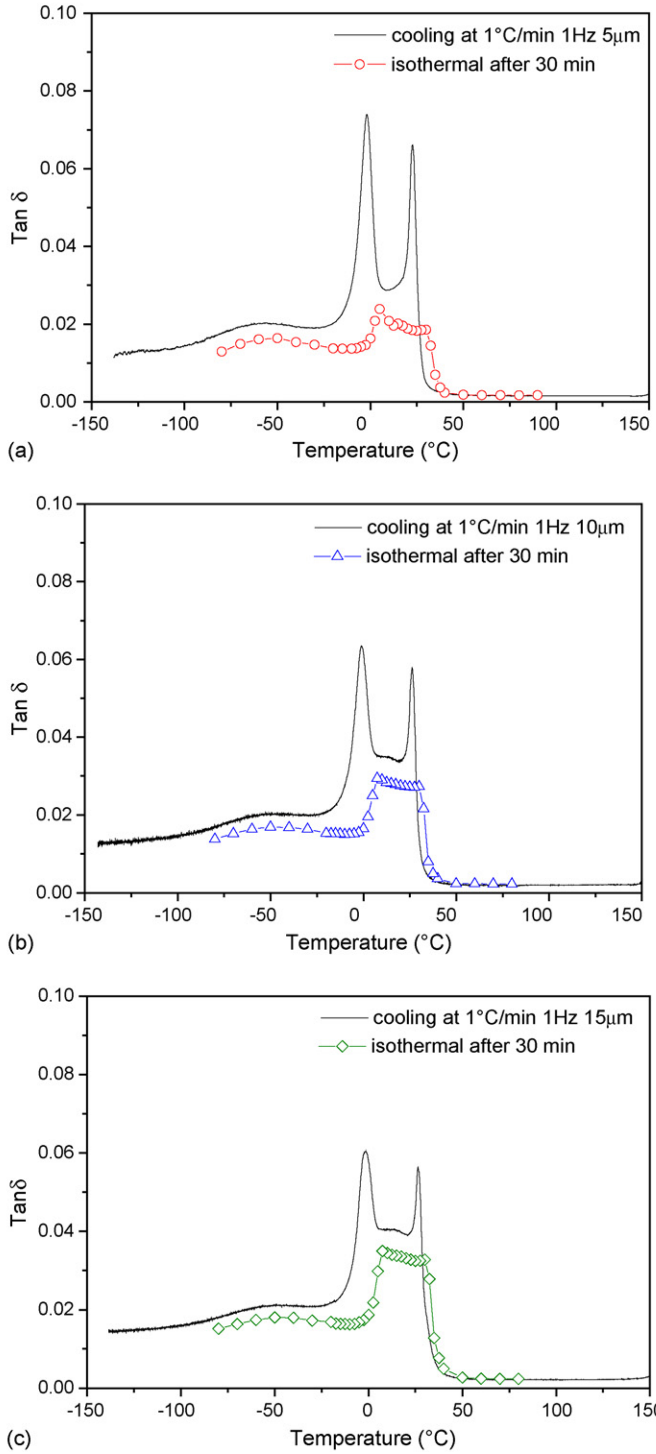

Fig. 5. The intrinsic $\tan\delta$ curves measured under isothermal conditions at $\dot{T}=1\,^{\circ}\mathrm{C/min}$ and $\upsilon = 1$ Hz with different amplitudes of (a) $\sigma_0 = 5$ μm (empty circle curve); (b) $\sigma_0 = 10$ μm (empty triangle curve); and (c) $\sigma_0 = 15$ μm (empty diamond curve).

ture indicates that the $\tan\delta$ values of IF_S^R and $IF_S^{B19'}$ are both independent of $\dot{T}$. Fig. 7(b) and (c) plot the $\tan\delta$ values of IF_S^R and $IF_S^{B19'}$ as a function of $1/\upsilon^{1/2}$ and σ_0 measured at 20 °C and −20 °C, respectively, in Figs. 4 and 5. As seen in Fig. 7, both IF_S^R and $IF_S^{B19'}$ are linearly proportional to $\sigma_0/\upsilon^{1/2}$ but independent of $\dot{T}$ when the applied υ and σ_0 are in between

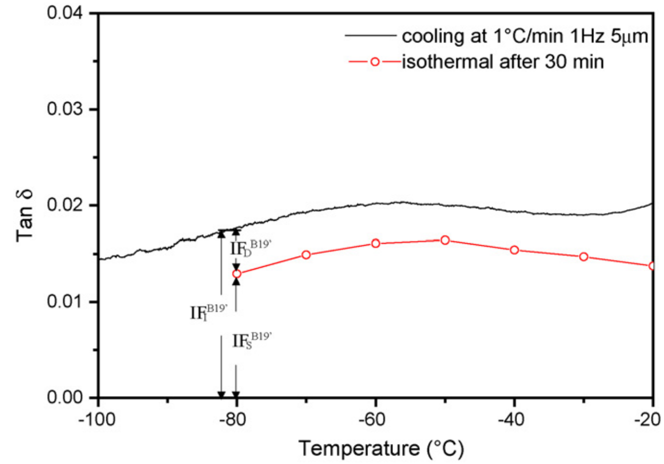

Fig. 6. Enlarged diagram of B19′ martensite region in Fig. 3(a).

0.1–10 Hz and 1–15 μm, respectively. This behavior is same as the damping characteristic of the inherent internal friction $IF_{PT} + IF_I$ of B2 → R and R → B19′ martensitic transformations which is also linearly proportional to $\sigma_0/\upsilon^{1/2}$ and independent of $\dot{T}$ [18]. Therefore, the inherent internal friction $IF_{PT} + IF_I$ of B2 → R and R → B19′ martensitic transformations and IF_S of the single R-phase and B19′ martensite may originate from the similar damping mechanism. Since the inherent internal friction $IF_{PT} + IF_I$ is mainly generated from stress-assisted martensitic transformation and stress-assisted motions of twin boundaries [18], the damping mechanism of IF_S^R and $IF_S^{B19'}$ is proposed to be contributed by the stress-assisted movements of twin boundaries in between the variants of R-phase and B19′ martensite, respectively.

From Figs. 3–5, all the measured $\tan\delta$ values of IF_S^{B2} are quite low and very close to those of IF_I^{B2}. This feature indicates that IF_I^{B2} is mainly contributed by the IF_S^{B2} while IF_D^{B2} is insignificant in B2 parent phase. Also from Figs. 3–5, both $\tan\delta$ values of IF_S^R and $IF_S^{B19'}$ are much higher than those of IF_S^{B2}. IF_S^{B2} exhibits a rather small intrinsic internal friction because its $\tan\delta$ only comes from the dynamic/static hysteresis of lattice defects [5]. On the other hand, from DMA results shown in Figs. 3–5, both IF_S^R and $IF_S^{B19'}$ have higher $\tan\delta$ values than those of IF_S^{B2} due to their abundant twin boundaries in between the variants which can be easily moved by the external stress to accommodate the applied strain. This characteristic indicates that the effect of twin boundaries on internal friction is more dominant than that of the lattice defects/dislocations introduced by cold-rolled and annealed treatment. Since the internal friction of IF_S^R and $IF_S^{B19'}$ are mainly contributed by stress-assisted motions of twin boundaries, the effect of defects/dislocations due to thermal/mechanical process on damping behavior can be neglected in this study. Furthermore, Figs. 3–5 also show that the $\tan\delta$ values of IF_S^R are always higher than those of $IF_S^{B19'}$ measured at the same experimental parameter. This feature comes from the fact that the lower storage modulus E_0 in R-phase, as shown in Fig. 1, leads to the easier movement of twin boundaries in R-phase and hence dissipates more energy during damping than B19′ martensite.

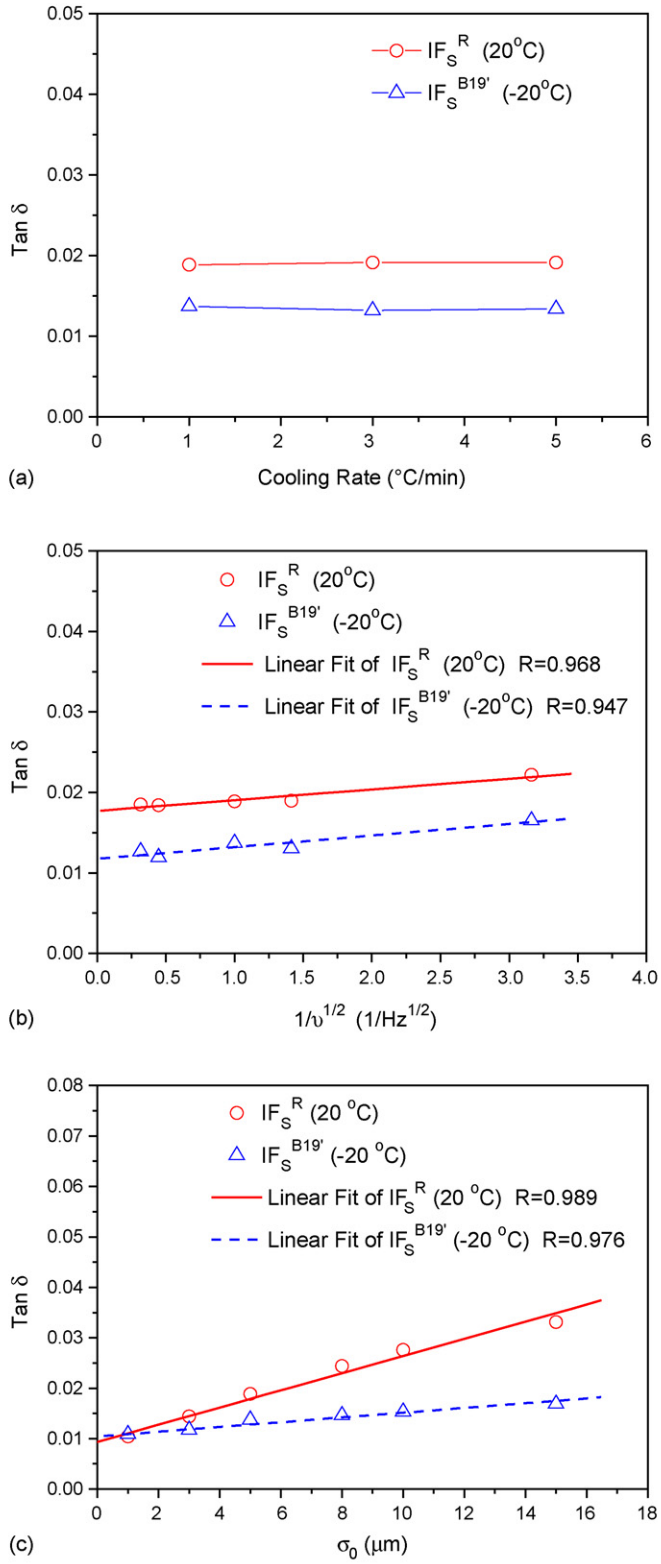

Fig. 7. The tan δ values of IF_S^R and $IF_S^{B19'}$ measured in Figs. 3–5 at 20 °C and −20 °C as a function of (a) $\dot{T}$; (b) $1/\upsilon^{1/2}$; and (c) σ_0.

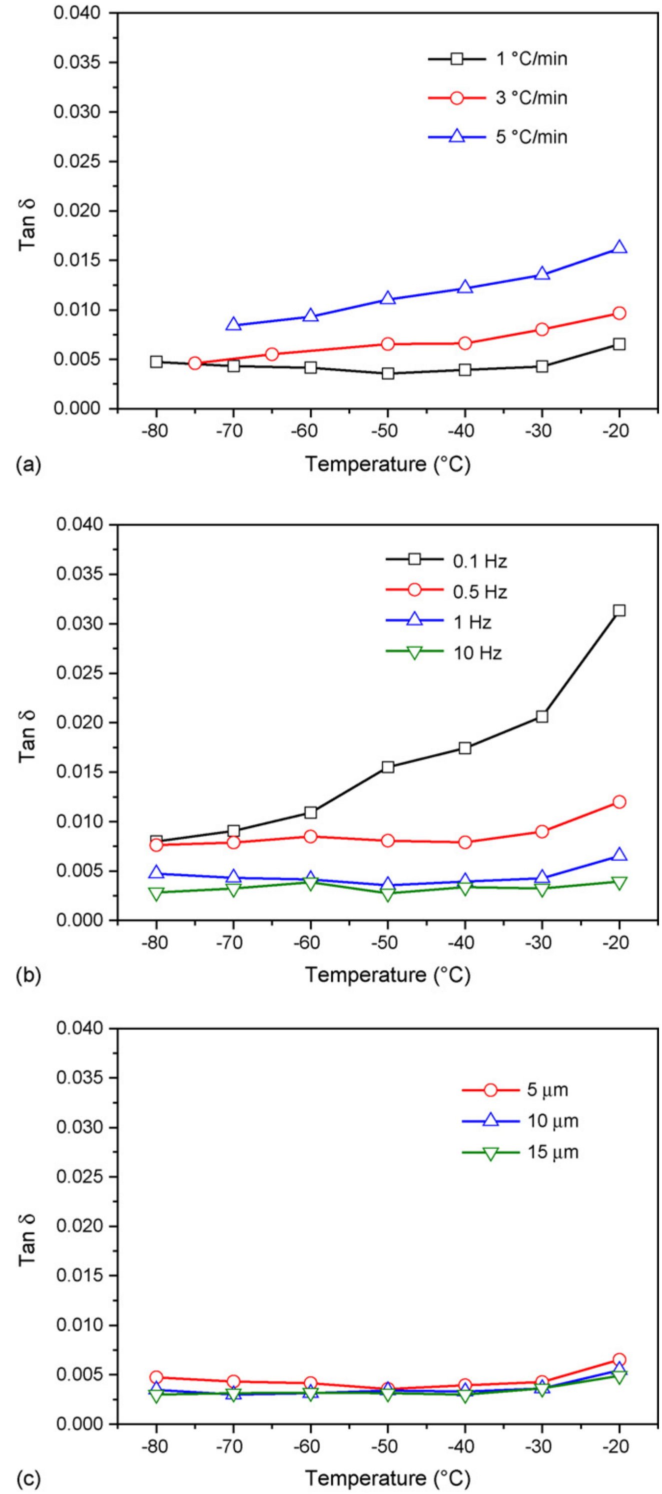

Fig. 8. The tan δ values of $IF_D^{B19'}$ vs. temperature obtained at (a) different $\dot{T}$ in Fig. 3; (b) different υ in Fig. 4; and (c) different σ_0 in Fig. 5.

4.2. IF_D of B19′ martensite

As illustrated in Fig. 6, when the specimen is kept isothermally at B19′ martensite, the decayed tan δ value represents the $IF_D^{B19'}$. The damping behavior of IF_D^R is suggested to be similar to that of $IF_D^{B19'}$, but IF_D^R damping is difficult to measure due to the R-phase having a narrow existing temperature range, as shown in Fig. 1. As a result, only $IF_D^{B19'}$ is discussed in detail in the following.

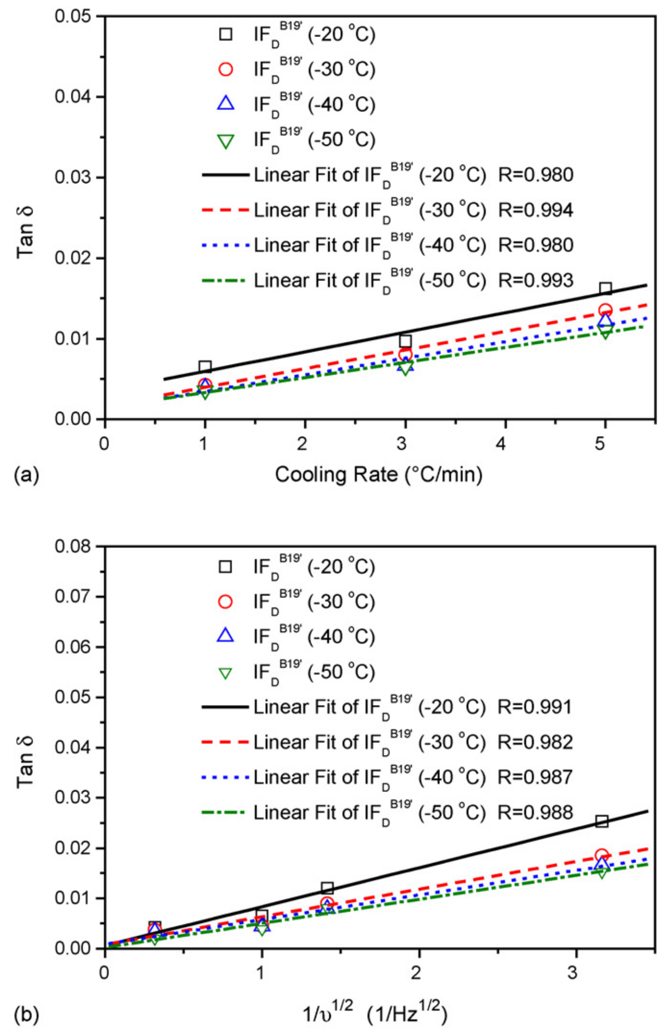

Fig. 9. The tan δ values of $IF_D^{B19'}$ measured in Fig. 8(a) and (b) at −20 °C, −30 °C, −40 °C and −50 °C as a function of (a) $\dot{T}$ and (b) $1/\upsilon^{1/2}$.

Fig. 8(a) plots the tan δ values of $IF_D^{B19'}$ versus. temperature in which $IF_D^{B19'}$ is calculated by subtracting $IF_S^{B19'}$ from $IF_I B19'$ measured at different $\dot{T}$ in Figs. 3 and 6. The temperature deviation of $IF_S^{B19'}$ and $IF_I B19'$ has been corrected by the peak temperature shift of R → B19′ transformation to eliminate the influence of $\dot{T}$. Fig. 8(b) and (c) show the tan δ values of $IF_D^{B19'}$ as a function of temperature at different υ measured in Fig. 4 and at different σ_0 measured in Fig. 5, respectively. As shown in Fig. 8, the tan δ values of $IF_D^{B19'}$ increase with $\dot{T}$ but decreases with υ and almost independent of σ_0. Fig. 9(a) and (b) plot the tan δ values of $IF_D^{B19'}$ as a function of $\dot{T}$ and $1/\upsilon^{1/2}$, respectively, in which $IF_D^{B19'}$ is measured at different temperatures (−20 °C, −30 °C, −40 °C and −50 °C). As shown in Figs. 8(c) and 9, all the tan δ values of $IF_D^{B19'}$ measured at different temperatures increase linearly with increasing $\dot{T}/\upsilon^{1/2}$ but independent of σ_0 when the applied $\dot{T}$ and υ are in between 1–5 °C/min and 0.1–10 Hz, respectively. This relationship is quite similar to that of IF_S^R and $IF_S^{B19'}$ except that the term σ_0 is now replaced by $\dot{T}$. This feature demonstrates that the damping mechanism of IF_S is generated by stress-assisted movements of twin boundaries while that of IF_D is contributed by thermal-assisted motions of twin boundaries. Furthermore, Fig. 8 shows $IF_D^{B19'}$ does not exhibit a broad peak at around −60 °C as $IF_S^{B19'}$ shown in Figs. 3–5. This indicates the occurrence of relaxation peak only comes from the $IF_S^{B19'}$, instead of the $IF_D^{B19'}$.

5. Conclusions

The intrinsic internal friction IF_I of R-phase and B19′ martensite measured at constant $\dot{T}$ is both composed of a static term IF_S which keeps steady after isothermal conditions and a dynamic term IF_D which diminishes during isothermal conditions. Both tan δ values of IF_S^R and $IF_S^{B19'}$ are linearly proportional to $\sigma_0/\upsilon^{1/2}$ when the applied υ and σ_0 are in between 0.1–10 Hz and 1–15 μm, respectively. Consequently, the damping mechanism of IF_S^R and $IF_S^{B19'}$ is associated with stress-assisted movements of twin boundaries in between the variants of R-phase and B19′ martensite, respectively. The tan δ value of IF_S^R is higher than that of $IF_S^{B19'}$ because the R-phase has softer storage modulus E_0 which leads to easier movement of twin boundaries in R-phase and dissipates more energy during damping. The tan δ value of $IF_D^{B19'}$ increases linearly with $\dot{T}/\upsilon^{1/2}$ and is independent of σ_0 when the applied $\dot{T}$ and υ are in between 1–5 °C/min and 0.1–10 Hz, respectively. It implies that the damping mechanism of IF_D^R is due to thermal-assisted motions, instead of stress-assisted movements, of twin boundaries in B19′ martensite. The occurrence of relaxation peak at about −60 °C only comes from the $IF_S^{B19'}$, instead of the $IF_D^{B19'}$.

Acknowledgement

The authors gratefully acknowledge the financial support for this research provided by the National Science Council (NSC), Taiwan, Republic of China, under Grants Nos. NSC94-2216-E002-030.

References

[1] C.M. Wayman, T.W. During, in: T.W. During, K.N. Melton, D. Stöckel, C.M. Wayman (Eds.), Engineering Aspects of Shape Memory Alloys, Butterworth-Heinemam, London, 1990, pp. 3–20.
[2] K. Iwasaki, R. Hasiguti, Trans. JIM 28 (1987) 363.
[3] O. Mercier, K.N. Melton, Y. De Préville, Acta Metall. 27 (1979) 1467.
[4] S.K. Wu, H.C. Lin, T.S. Chou, Acta Metall. 38 (1990) 95.
[5] H.C. Lin, S.K. Wu, M.T. Yeh, Metall. Mater. Trans. A 24 (1993) 2189.
[6] K. Sugimoto, T. Mori, K. Otsuka, K. Shimizu, Scripta Metall. 8 (1974) 1341.
[7] Y. Liu, J. Van Humbeeck, R. Stalmans, L. Delaey, J. Alloys Compd. 247 (1997) 115.
[8] B. Coluzzi, A. Biscarini, R. Campanella, L. Trotta, G. Mazzolai, A. Tuissi, F.M. Mazzolai, Acta Mater. 47 (1999) 1965.
[9] S.K. Wu, H.C. Lin, J. Alloys Compd. 72–78 (2003) 355.
[10] S.H. Chang, S.K. Wu, Key Eng. Mater. 319 (2006) 9.
[11] J.F. Delorme, R. Schmid, M. Robin, P. Gobin, J. Phys. 32 (1971) C2–C101.

[12] W. Dejonghe, R. De Batist, L. Delaey, Scripta Metall. 10 (1976) 1125.
[13] J.E. Bidaux, R. Schaller, W. Benoit, J. Phys. 46 (1985) C10–C601.
[14] J. Van Humbeek, J. Stoiber, L. Delaey, R. Gotthardt, Z. Metallkd. 86 (1995) 1976.
[15] J.S. Zhu, R. Schaller, W. Benoit, Phys. Stat. Sol. A 108 (1988) 613.
[16] G. Gremaud, J.E. Bidaux, W. Benoit, Helv. Physica Acta 60 (1987) 947.
[17] J.E. Bidaux, R. Schaller, W. Benoit, Acta Metall. 37 (1989) 803.
[18] S.H. Chang, S.K. Wu, Scripta Mater. 55 (2006) 311.
[19] S.H. Chang, S.K. Wu, Scripta Mater. 50 (2004) 937.